ELSEVIER

Earth and Planetary Science Letters 186 (2001) 57–73

EPSL

www.elsevier.com/locate/epsl

Along-strike variations in the thermal and tectonic response of the continental Ecuadorian Andes to the collision with heterogeneous oceanic crust

R.A. Spikings [a,*], W. Winkler [a], D. Seward [a], R. Handler [b]

[a] *Geologisches Institut, ETH Zentrum, CH-8092 Zurich, Switzerland*
[b] *Institute for Geology and Palaeontology, University of Salzburg, Hellbrunner Str. 34/III, A-5020 Salzburg, Austria*

Received 24 July 2000; accepted 29 December 2000

Abstract

Oblique to strike geological segmentation in the Andean chain has been previously recognised at various scales and is commonly attributed to changes in the convergence vectors of the oceanic and continental plates, as well as the upper-plate expressions of differing along-strike subducted slab age, strength and composition. We present new white mica and biotite $^{40}Ar/^{39}Ar$ and zircon and apatite fission-track data from several traverses across the Cordillera Real of Ecuador in the northern Andes that reveal distinct along-strike differences in the timing of accelerated crustal cooling during the Cenozoic. The data record elevated cooling rates from temperatures of ~380°C during ~65–55 and ~43–30 Ma from all sampled regions of the Cordillera Real and at ~15 Ma and since ~9 Ma in the northern Cordillera Real. Each cooling period was probably driven by exhumation in response to the accretion and subduction of heterogeneous oceanic crust. Elevated cooling rates of up to ~30–20°C/Myr were initiated during the Palaeocene and Eocene–early Oligocene along the entire contemporaneous margin of Ecuador and were driven by the accretion of the oceanic Pallatanga Terrane and Piñon–Macuchi Block, respectively, onto northwestern South America. Both of these geological provinces originated at the southern parts of the leading and trailing boundaries of the Caribbean Plateau and accreted onto the margin during the approximately northeastward migration of the Plateau into its current position. Within Ecuador the development of higher topography and elevated cooling rates of up to 50°C/Myr at ~15 Ma and since ~9 Ma are restricted to the region north of 1°30′S and is situated above the postulated subducted flat-slab section of the aseismic Carnegie Ridge. Plate convergence rate calculations suggest the Carnegie Ridge collided with the Ecuador Trench at ~15 Ma, which caused the pre-existing coastal provinces to displace to the northeast, subsequently driving extension and marine ingressions in southern Ecuador and compression and uplift in northern Ecuador.

Keywords: Northern Andes; Ecuador; Carnegie Ridge; Caribbean Plate; thermochronology; tectonics

1. Introduction

North–south, oblique to strike geological segmentation in the Andean chain has been identified

* Corresponding author. Fax: +41-1632-1080; E-mail: richard.spikings@erdw.ethz.ch

0012-821X/01/$ – see front matter
PII: S0012-821X(01)00225-4

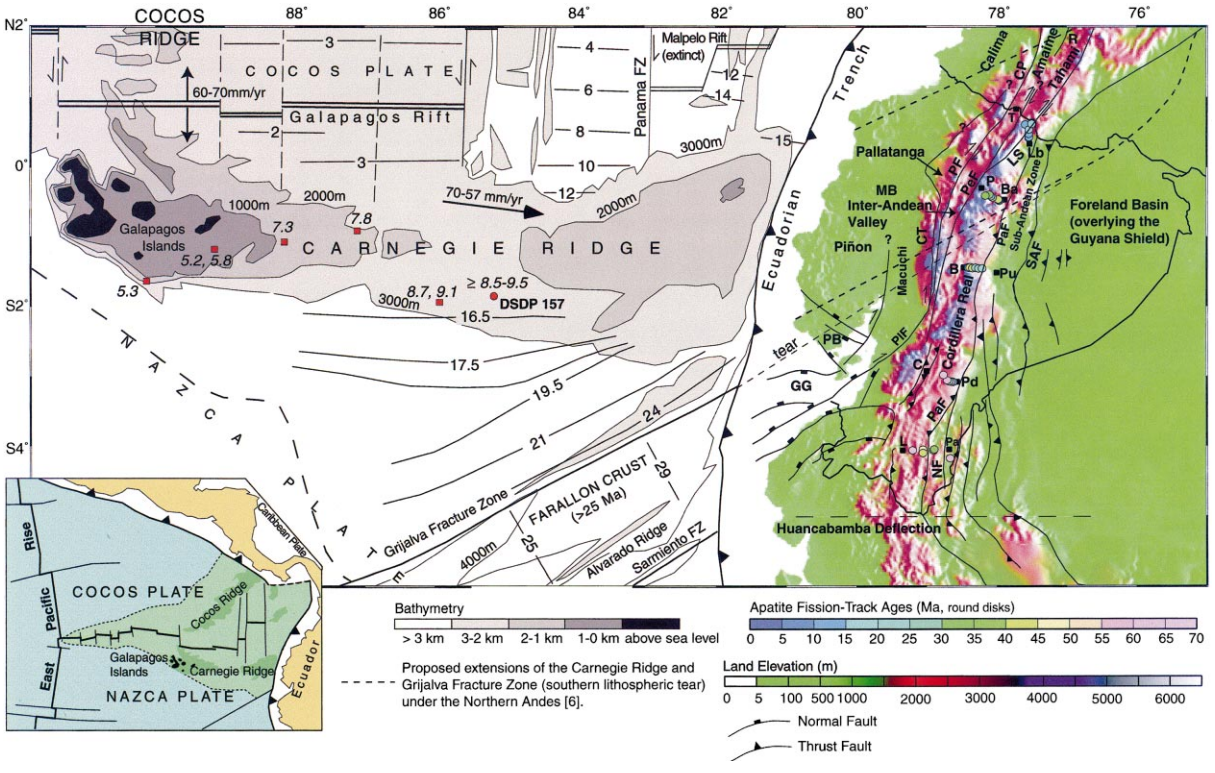

Fig. 1. Digital elevation model of the Ecuadorian Andes (GTOPO30) with illumination from the east. Colour coded AFT ages from five traverses across the Cordillera Real are shown (from north to south: Tulcan (T)–La Bonita (Lb), Papallacta (P)–Baeza (Ba), Baños (B)–Puyo (Pu), Cuenca (C)–Plan del Milagro (Pd), Loja (L)–Paquisha (Pa)). Young AFT ages are recorded in the Andean belt situated above the proposed extension of the Carnegie Ridge [6] and Grijalva Fracture Zone representing a buoyant oceanic slab compared to the remnants of the Farallon Plate. The elevated landscape swings seaward in the vicinity of the Gulf of Guayaquil. Simplified bathymetry, magnetic anomalies (approximate age in Ma) [6,40] and plate vectors [16] of the Nazca Plate are shown. Red symbols indicate the position of dredged and dated Galapagos Hot Spot basalts [47] and biostratigraphically dated sediments (9.5–8.5 Ma), which lie on hot spot basalts at the DSDP Site 157 [48]. Inset shows the oceanic crust (light green) and Galapagos Hot Spot ridges (dark green) that have formed since ~25 Ma. Abbreviations: CP, Cauca Fault; CT, Chimbo–Toachi Shear Zone; GG, Gulf of Guayaquil; LS, La Sofia Fault; MB, Manabi Basin; NF, Nangaritza Fault; PB, Progresso Basin; PaF, Palanda Fault; PeF, Peltetec Fault; PF, Pujili Fault; PlF, Pallatanga Fault; R, Romeral Fault; SAF, Sub-Andean Fault.

at various scales for at least 30 yr (e.g. [1,2]) and three Andean segments (northern, central and southern) are traditionally recognised. Documented geological variations include geomorphological changes in the height and width of the Andean Range (Fig. 1), distinct changes in 20th century seismicity [3], the timing of Neogene volcanic activity and differences in volcanic arc width [4] and composition [5]. Along-strike variations are generally related to changes in the convergence vectors of the oceanic and continental plates, as well as upper-plate expressions of differing along-strike subducted slab age, strength and composition (e.g. [6]).

The Ecuadorian continental margin, situated in the northern Andean segment (north of 5°S), is separated from the central segment by a distinct change in the convergence angle between the oceanic Nazca and the South American (SOAM) coast line [1], otherwise referred to as the Huancabamba Deflection (Fig. 1). Subduction of heterogeneous oceanic crust beneath both the continental margin and accreted oceanic plateau material has occurred since the late Middle Juras-

sic (~160 Ma), initially within the Tethyan spreading system and afterwards in the Eastern Pacific subduction system [7–9]. The accretion of allochthonous terranes onto the Guyana Shield at ~140–120 Ma during the Peltetec Event [10] resulted in crustal thickening, cratonward propagation and building of the Cordillera Real onto the continental margin of Ecuador since that time (e.g. [10]). Unroofing of the Cordillera has exposed poly-deformed, greenschist facies and lower grade metamorphic rocks (e.g. [10,11]).

Oceanic hotspot activity, plate rearrangements and the generation of new spreading centres since at least 80 Ma has resulted in large structural, thickness and density heterogeneities in the approaching and subducting oceanic slab parallel to the northern segment (Fig. 1). These include: (1) the obduction of ophiolites and the accretion of allochthonous terranes, composed of anomalously thick (>10 km) oceanic plateau material onto the continental margin during the Late Cretaceous–Early Tertiary (e.g. [12]; (2) the break-up of the Farallon Plate into the Nazca and Cocos plates and a change of the subducting plate vector at the Ecuador Trench from east-northeast to east at ~25 Ma [7,8] and (3) subduction and upper–lower plate coupling of the buoyant aseismic Carnegie Ridge since the late Miocene [6]. Numerous models exist that speculate on the response of the upper-plate to changes in the properties of the colliding oceanic plate (e.g. [6]).

We present the results of $^{40}Ar/^{39}Ar$ (white mica and biotite) analyses and zircon and apatite fission-track (ZFT and AFT) analyses from traverses across the Cordillera Real of the Ecuadorian Andes. Each of the minerals studied provides thermal history information over a given temperature range and when the results are integrated they can yield temperature–time paths. The resultant thermal histories permit an assessment of the timing, magnitude and duration of thermal events over the temperature range of ~380–60°C, and may help to define the responsible geological processes. In this context a quantitative framework for the thermal and exhumation history of the Cordillera Real during the Cenozoic has been established. The framework provides constraints on the unroofing history of the continental margin and reveals systematic distinctive approximately north–south oriented, along-strike trends, which can be compared with contemporaneous heterogeneities in the approaching and subducting oceanic crust.

2. Geological framework

Early Cretaceous to Recent convergence between the Pacific oceanic and SOAM plates has given rise to a series of distinguishable tectono-stratigraphic regions (Fig. 1), which for the purposes of this contribution are divided into an oceanic and a continental province. The continental province is partly comprised of a supra-crustal sequence of Palaeozoic–Lower Cretaceous metamorphic rocks of the Cordillera Real, which together with Cretaceous and Tertiary sediments of the retro-arc Amazon Foreland Basin (Fig. 1) unconformably overlie the continental, sub-crustal, Precambrian Guyana Shield. The Cordillera Real continues northwards into Colombia and is believed to be composed of a series of sublinear tectono-stratigraphic belts, which are referred to as the Alao, Loja and Salado terranes [10]. Oligocene and Miocene ignimbrities, exposed in the Inter-Andean Valley (Fig. 1), obscure the western limit of metamorphic rocks that form the Cordillera Real. However, negative Bouguer anomalies extend westward from the Cordillera across the valley [13] and it is likely that rocks of the Cordillera Real form the basement in the Inter-Andean Valley. Alternatively, the existence of a separate microplate beneath the valley has been postulated [10].

Immediately to the east of the Cordillera Real the proximal Amazon Foreland Basin is composed of steeply dipping thrust slices and large antiforms within a series of foothill highs, which are commonly referred to as the Sub-Andean Zone (SAZ; Fig. 1). Within the SAZ, conspicuous tectonic uplift is evident exposing Palaeozoic to Tertiary basement, cover and foreland basin formations.

The oceanic province consists of three distinguishable major allochthonous oceanic terranes [14], which are thought to have accreted to the

continental margin in two stages. The timing and order of accretion of these terranes is still a subject of debate although Hughes and Pilatasig [12] suggest the first collision occurred between the oceanic Pallatanga Terrane (Early–Late Cretaceous MOR basalts and peridotites) and the continental margin between 85 and 65 Ma (Fig. 1). The second stage of accretion involved the collision of the oceanic Late Cretaceous–Early Eocene composite Piñon–Macuchi Block with the Pallatanga Terrane within a dextral shear regime along the Chimbo–Toachi Shear Zone (Fig. 1; [12]). A middle to Late Eocene marine turbidite sequence is common to both the Piñon–Macuchi Block and the Pallatanga Terrane [12] suggesting that they had accreted together by this time.

The suture between the oceanic and continental provinces is defined by a tectonic melange, which hosts metre scale blocks of metamorphic rocks of the Cordillera Real [12]. This feature is locally referred to as the Pujili Fault and extends southwards where it intersects the Pallatanga Fault, which is commonly thought to intersect the Ecuador Trench in the region of the Gulf of Guayaquil (Fig. 1). The suture continues northwards into Colombia where it is referred to as the Cauca–Romeral Fault System (e.g. [15]) and marks a distinct increase of 275 mgal in the Bouguer anomalies traversing from east to west. At present, almost orthogonal subduction of the Nazca Plate beneath the SOAM Plate is occurring along the Ecuadorian section of the boundary at a convergence rate of 70–57 mm/yr [16,17].

3. Methods and results

Spikings et al. [18] presented ZFT and AFT data from three traverses across the Cordillera Real of Ecuador north of 1°30′S (Fig. 1). Their results constrain the timing and amount of cooling and exhumation of regions of the northern Cordillera Real through a static geothermal gradient. In this contribution, we present new $^{40}Ar/^{39}Ar$ data from white mica and biotite from those same traverses (Table 1). In addition, 26 ZFT and AFT ages are presented from two traverses south of 2°30′S, which are oriented approximately per-

Table 1
$^{40}Ar/^{39}Ar$ age data from north of 1°30′S

Sample	Lithology, formation, region	Latitude	Longitude	Age ± 1σ (Ma)
White mica:				
98RS19	muscovite gneiss, TL granite, lo	0°21′43″S	78°05′10″W	66 ± 1 (P)
98RS26b	Hbl granodiorite, Azafran granite, sa	01°24′02″S	78°20′41″W	56 ± 1 (P)
98RS27	muscovite granite, Azafran granite, sa	01°24′02″S	78°20′41″W	59 ± 1 (P)
Biotite:				
98RS14	graphitic mica schist, Upano Unit, sa	0°26′10″S	77°57′36″W	62 ± 1 (TFA)
98RS26b	Hbl granodiorite, Azafran granite, sa	01°24′02″S	78°20′41″W	58 ± 1 (P)
98RS33	Bt schist, Azafran granite, sa	01°24′10″S	78°19′34″W	62 ± 2 (P)
98RS55	rhyolite, Misahualli volcanics, SAZ	0°26′18″N	77°31′57″W	162 ± 2 (TFA)

lo, Loja Terrane; sa, Salado Terrane; SAZ, Sub-Andean Zone.

TFA: total fusion age, result of a single step total fusion experiment or total age derived from a step heating experiment. P: plateau age, quoted for those samples that have undergone a step heating experiment and have yielded a plateau region on the spectrum (concordant to 2σ). The age is the weighted mean age of the plateau. Correction factors for interfering isotopes are: $^{36}Ar/^{37}Ar(Ca) = 0.0003$, $^{39}Ar/^{37}Ar(Ca) = 0.00065$ and $^{40}Ar/^{39}Ar(K) = 0.03$. Variations in the neutron flux were monitored with the B4M white mica standard for which a $^{40}Ar/^{39}Ar$ plateau age of 18.6 ± 0.4 Ma has been reported [21]. $^{40}Ar/^{39}Ar$ analyses were carried out using a UHV Ar-extraction line equipped with a Merchantek™ UV/IR laser ablation facility, and a VG-Isotech™ NG3600 mass spectrometer. Stepwise heating analyses of samples were performed using a PC controlled defocused 25 W CO_2-IR laser. The extracted gas was passed across one hot and one cold Zr–Al SAES getter and transferred into a bright Nier-type source operating at 4.5 kV. Measurements were recorded by an axial electron multiplier in static mode. ^{36}Ar, ^{37}Ar, ^{38}Ar, ^{39}Ar and ^{40}Ar isotope intensities were corrected for system blanks, background, post-irradiation decay of ^{37}Ar and interfering isotopes.

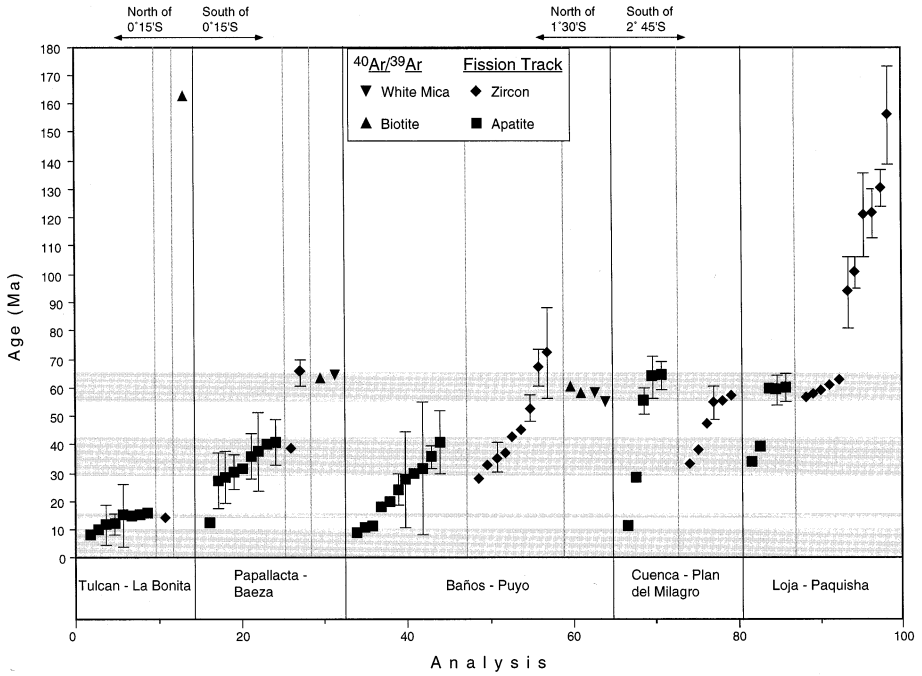

Fig. 2. A compilation of white mica and biotite $^{40}Ar/^{39}Ar$ and ZFT and AFT ages ($\pm 1\sigma$ error) from five traverses across the Cordillera Real of Ecuador; including those from north of 1°30′S [18]. Horizontal shaded bars highlight those time periods when regional scale exhumation was occurring at its greatest rates (see Section 4). Fission-track data for samples north of 1°30′S are from Spikings et al. [18].

pendicular to the Andean trend and structural strike. The complete data set, including the ages of Spikings et al. [18] is illustrated in Fig. 2.

Mineral separates for both the $^{40}Ar/^{39}Ar$ and fission-track methods were extracted from whole rock specimens using conventional magnetic and heavy liquid methods. For $^{40}Ar/^{39}Ar$ dating sealed quartz vials containing the target minerals were irradiated in the central position of the ASTRA reactor at the Austrian Research Center for 8 h with an average neutron flux of 8×10^{13} n/cm^2. Ages and errors were calculated following suggestions by McDougall and Harrison [19] using the decay constants of Steiger and Jäger [20] (Table 1).

The external detector method was used to determine the fission-track ages of all samples in this study (see [18] for a more detailed description of the analytical method; Table 2). When the single grain ages for a particular sample yielded a $P(\chi^2)$ parameter of $<5\%$ it was assumed that more than one age population is present. Individual age populations have been resolved [22] and the ages of all populations are presented in Table 2.

3.1. $^{40}Ar/^{39}Ar$ ages north of 1°30′S

Step heating of white mica from the Triassic (228 ± 3 Ma U/Pb zircon age [10]) Tres Lagunas Granite 98RS19 near to the town of Papallacta in northern Ecuador yielded a plateau age of 66 ± 1 Ma (Table 1; Figs. 1 and 2). Further south, two white micas from the Azafran Granite (143 ± 1 Ma U/Pb zircon age [10]), located between the towns of Baños and Puyo (Fig. 1), yielded plateau ages of 59 ± 1 and 56 ± 1 Ma. These ages are concordant (within error limits) to several ZFT ages reported from the same regions [18] (Fig. 2).

Biotite 98RS55 (rhyolite) taken from a deformed sequence of the ill-defined Jurassic Misahualli Volcanics Unit between the towns of Tulcan and La Bonita yielded a slightly disturbed age

Table 2
AFT and ZFT data from south of 2°45′, Cordillera Real, Ecuador

Sample No.	Stratigraphic unit/terrane	Lithology	Latitude (S)	Longitude (W)	Altitude (m)	No. of grains	Standard track density × 10^6	Spontaneous track density × 10^6	Induced track density × 10^6	$P(\chi^2)$ (%)	U (ppm)	Fission-track age ± 1 σ (Ma)	Mean track length ± 1σ (μm)	Standard deviation (μm)
Apatite:														
Cuenca–Plan del Milagro														
99RS53	Chiguinda Unit, lo	sandy quartzite	03°00′45″	78°35′56″	2700	21	1.030 (5467)	0.1713 (110)	3.168 (2034)	73	38	10.8 ± 1.2		
99RS55	Chiguinda Unit, lo	biotite schist	03°00′09″	78°39′15″	3380	21	1.170 (5467)	0.6397 (689)	5.285 (5692)	9	57	27.9 ± 1.9	13.49 ± 0.27 (29)	1.43
99RS56	TL granite, lo	granite	02°59′13″	78°40′51″	3375	18	1.100 (5189)	1.176 (1231)	4.966 (5199)	6	56	55.2 ± 4.8	13.23 ± 0.17 (69)	1.38
99RS59	Alao-Paute Unit, al	schist	02°54′49″	78°44′07″	2750	22	1.068 (5467)	0.3196 (317)	1.025 (1017)	26	12	64.1 ± 5.1	12.72 ± 0.36 (9)	1.08
Loja–Paquisha														
99RS37	Chiguinda Unit, lo	phyllite	03°59′01″	79°10′02″	2670	26	1.081 (5467)	1.006 (995)	3.526 (3487)	5	41	59.6 ± 2.9	13.26 ± 0.27 (55)	1.97
99RS40	Sabanilla migmatite, lo	granodiorite	03°58′15″	79°01′17″	1975	20	1.045 (5189)	1.369 (1715)	6.104 (7648)	7	73	45.0 ± 2.0	13.19 ± 0.15 (100)	1.45
99RS41	Sabanilla migmatite, lo	migmatite	04°01′05″	79°01′20″	1500	20	1.003 (5189)	1.813 (2165)	9.039 (10792)	10	113	39.5 ± 2.0	12.53 ± 0.15 (164)	1.9
99RS42	Zamora batholith, SAZ	granodiorite	03°59′02″	78°52′18″	980	25	1.093 (5467)	0.2436 (344)	0.9207 (1300)	12	11	59.6 ± 5.0	13.58 ± 0.31 (26)	1.56
99RS43	Zamora batholith, SAZ	coarse granite	03°58′07″	78°51′46″	875	13	1.141 (5189)	0.3250 (156)	2.106 (1011)	82	23	34.0 ± 3.3	12.56 ± 0.48 (16)	1.92
99RS47	Zamora batholith, SAZ	Hbl phyric granite	04°05′33″	78°38′23″	800	25	0.9480 (5189)	0.1485 (263)	0.4483 (794)	11	6	60.5 ± 5.1	13.31 ± 0.25 (50)	1.76
Zircon:														
Cuenca–Plan del Milagro														
99RS51	Upano Unit, sa	graphitic phyllite	03°00′02″	78°30′34″	3050	25	3.404 (2219)	4.648 (998)	2.757 (592)	40	324	38.5 ± 2.3		
99RS52*	Chiguinda Unit?, lo	mica schist	03°00′07″	78°33′25″	2500	7	4.489 (2606)	5.682 (253)	3.121 (139)	85	278	54.8 ± 6.0		
99RS53	Chiguinda Unit, lo	sandy quartzite	03°00′45″	78°35′56″	2850	55	4.148 (2606)	9.609 (7180)	4.764 (3560)	6	459	57.6 ± 2.4		
99RS54	Ishpingo pluton, lo	diorite	03°00′30″	78°37′30″	3400	11	4.065 (2632)	9.252 (1140)	7.588 (935)	54	747	33.3 ± 1.8		
99RS55	Chiguinda Unit, lo	Bt pyritic schist	03°00′09″	78°39′15″	3375	16	4.636 (2606)	7.434 (1052)	4.162 (589)	16	359	55.5 ± 3.3		
99RS56	TL granite, lo	gneissic granite	02°59′13″	78°40′51″	3370	34	3.209 (2219)	9.101 (2909)	4.110 (1314)	65	512	47.6 ± 2.2		
Populations														
99RS52	Chiguinda Unit?, lo	mica schist	03°00′07″	78°33′25″	2500		4.489 (2606)	11.72 (143)	0.7377 (9)	100	66	463 ± 160		
Loja–Paquisha														
99RS37	Chiguinda Unit, lo	phyllite	03°59′01″	79°10′02″	2675	30	3.227 (2632)	6.928 (2096)	2.522 (763)	11	313	59.4 ± 3.1		
99RS38[a]	Chiguinda Unit, lo	micaceous quartzite	03°59′38″	79°08′22″	2775	26	4.051 (2606)	8.488 (3443)	4.4042 (1640)	43	399	57.0 ± 2.4		
99RS39[a]	Chiguinda Unit, lo	micaceous quartzite	03°59′15″	79°05′38″	2600	29	4.002 (2606)	8.832 (2737)	3.757 (1164)	6	376	63.0 ± 2.9		
99RS40	Sabanilla migmatite, lo	granodiorite	03°58′15″	79°01′17″	1975	23	3.456 (2632)	11.98 (1951)	4.789 (780)	42	554	57.9 ± 3.0		
99RS41	Sabanilla migmatite, lo	migmatite	04°01′05″	79°01′20″	1500	19	4.538 (2606)	8.438 (1575)	4.194 (783)	96	370	61.2 ± 3.3		
99RS43	Zamora batholith, SAZ	coarse granite	03°58′07″	78°51′46″	870	33	3.143 (2219)	11.17 (3312)	2.322 (688)	90	296	101.0 ± 5.3		
99RS46[a]	Hollin Fm., SAZ	quartz arenite	04°08′38″	78°37′58″	1000	3	3.684 (2632)	15.66 (430)	3.169 (87)	83	344	121 ± 15		
99RS47	Zamora batholith, SAZ	Hbl phyric granite	04°05′33″	78°38′23″	800	24	4.343 (2606)	9.676 (4486)	2.126 (986)	9	196	130.7 ± 6.4		
99RS48	Zamora batholith, SAZ	Hbl phyric granite	03°45′54″	78°43′32″	1000	20	3.912 (2632)	15.47 (1387)	3.301 (296)	33	338	122.2 ± 8.6		

Table 2 (*continued*)

Sample No.	Stratigraphic unit/terrane	Lithology	Latitude (S)	Longitude (W)	Altitude (m)	No. of grains	Standard track density $\times 10^6$	Spontaneous track density $\times 10^6$	Induced track density $\times 10^6$	$P(\chi^2)$ (%)	U (ppm)	Fission-track age $\pm 1\ \sigma$ (Ma)	Mean track length $\pm 1\sigma$ (μm)	Standard deviation (μm)
Populations														
99RS38	Chiguinda Unit, lo	micaceous quartzite	03°59′38″	79°08′22″	2775	1	4.051 (2606)	8.598 (257)	2.476 (74)	100	245	94 ± 13		
99RS39	Chiguinda Unit, lo	micaceous quartzite	03°59′15″	79°05′38″	2600	4	4.002 (2606)	17.34 (603)	2.951 (103)	39	295	156 ± 17		
99RS46	Hollin Fm., SAZ	quartz arenite	04°08′38″	78°37′58″	1000	31	3.684 (2632)	24.98 (2910)	1.738 (203)	36	189	347 ± 27		

Numbers in parentheses are the number of tracks counted, no track lengths are measured in the zircon crystals. When $P(\chi^2)$ is $< 5\%$ the fission-track age is the central age, otherwise it is the pooled age. Sample codes in bold type indicate those samples which yielded both AFT and ZFT ages. Bt, biotite; Hbl, hornblende. Al, Alao Terrane; lo, Loja Terrane; sa, Salado Terrane; SAZ, Sub-Andean Zone.

[a]Denotes sample which is comprised of > 1 source population (zircons only). The age of the older population is listed under '*Populations*'. All zircon and apatite separates were counted by R. Spikings using zeta calibration values of 387 ± 17 (apatite analysis, CN5 standard glass) and 134.7 ± 3.1 (zircon analysis, CN1 standard glass). Fossil tracks were revealed in apatites by etching in 5 N HNO_3 (aq.) at 20°C for 21 s and zircon by etching in the eutectic mixture of NaOH/KOH at 210°C for periods between 5 and 50 h. Induced tracks were revealed in muscovite external detectors by etching in 40% HF (aq.) at 20°C for 45 min.

spectrum with a total fusion age of 162 ± 2 Ma (Table 1). Biotite 98RS14 (graphitic schist) taken from the Late Jurassic Upano Unit between the towns of Papallacta and Baeza also yielded a disturbed age spectrum with a total fusion age of 62 ± 1 Ma. Finally, biotites from the Azafran Granite (143 ± 1 Ma U/Pb zircon age [10]) between the towns of Baños and Puyo yielded plateau ages of 62 ± 2 Ma (98RS33, granite) and 58 ± 1 Ma (98RS26b, granite; Table 1).

3.2. Fission-track ages south of 2°45′S

3.2.1. Cuenca–Plan del Milagro traverse

Rock samples were taken from different fault bounded units of Palaeozoic–Early Cretaceous rocks between the towns of Cuenca and Plan del Milagro (Fig. 1). AFT ages from this traverse range between ~64 and ~11 Ma (Table 2; Fig. 3). A majority of ZFT ages range between ~58 and ~33 Ma although sample 99RS52 (mica schist) from the Palaeozoic Chiguinda Unit yielded an older population of grains, which yielded a fission-track age of 463 ± 160 Ma (Table 2). The variation in the ages shows no geographic trend or linear correlation with altitude (Fig. 3). AFT mean lengths are partially annealed ranging between 13.23 and 13.49 μm (Fig. 4) with broad to medium standard deviations (Table 2).

3.2.2. Loja–Paquisha traverse

The traverse between the towns of Loja and Paquisha intersects the Loja Terrane of the Cordillera Real and crosses the Palanda Fault into the SAZ, extending across the Middle Jurassic Zamora Batholith (Rb/Sr and K/Ar ages range between 170 and 190 Ma [10]) and into sedimentary rocks of the Amazon Foreland Basin (Fig. 3).

Within the Loja Terrane, west of the Palanda Fault, a younger population of ZFT ages lies within a narrow range between 63 and 57 Ma (Fig. 2). However, micaceous quartzites from the Palaeozoic Chiguinda Unit contain older zircon populations (Table 2) with ZFT ages of 94 ± 13 Ma (99RS38) and 156 ± 17 Ma (99RS39). AFT ages from the Loja Terrane range between 60 and 40 Ma and have intermediate mean track lengths ranging between 12.53 and 13.26 μm (Fig. 4).

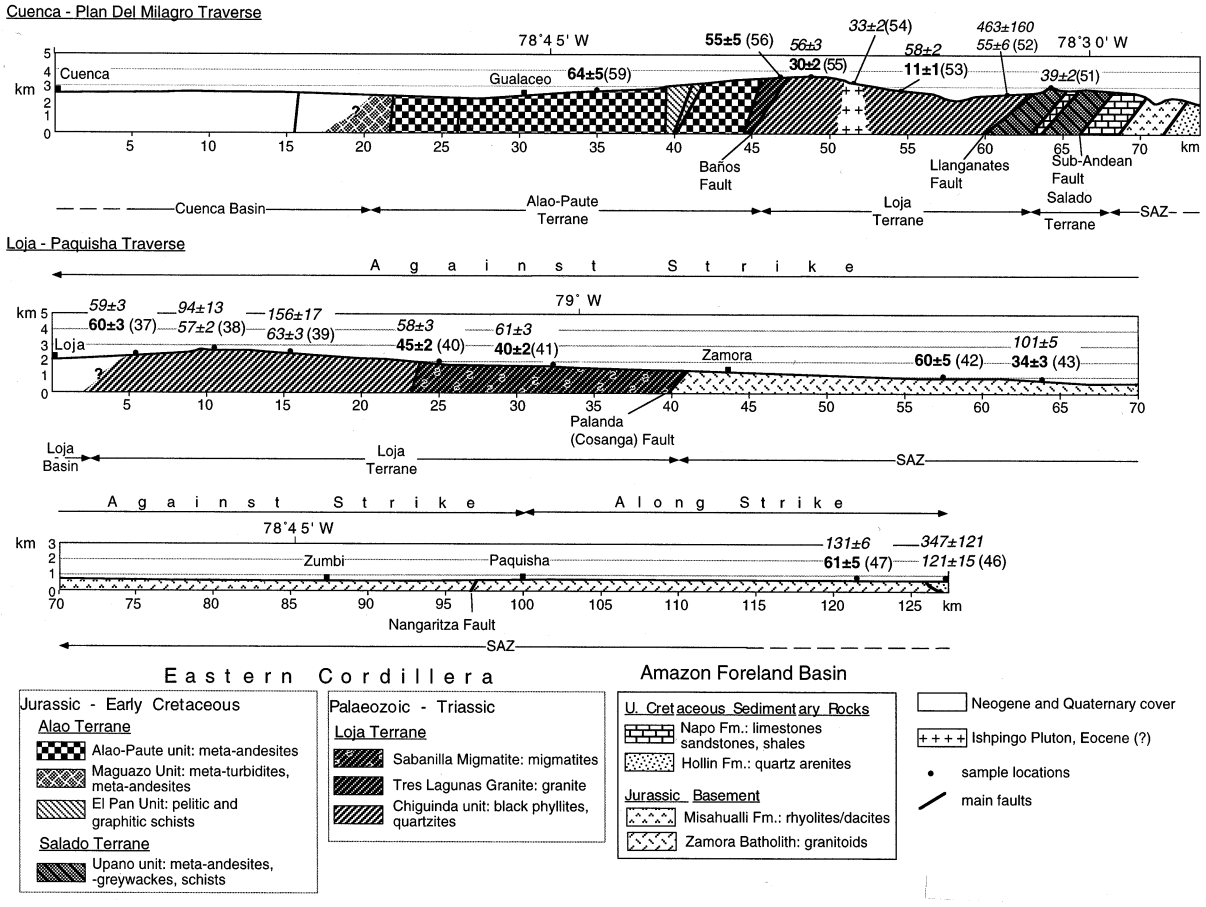

Fig. 3. Two simplified geological sections across the southern (south of 2°45′S) Cordillera Real, Ecuador [10]. The traverses correspond to those shown in Fig. 1 (Cuenca–Plan del Milagro, Loja–Paquisha). Fission-track ages are shown (italic = zircon; bold plain text = apatite) with sample numbers in brackets (see also Table 2). SAZ: Sub-Andean Zone.

The Zamora Batholith yields older ZFT ages ranging between ~131 and 101 Ma and are distinctly older to the east of the Nangaritza Fault (Figs. 1 and 3). AFT ages from the batholith are younger and lie between 60 and 34 Ma.

Finally, within the proximal SAZ, detrital zircon from a quartz arenite of the Hollin Formation (Fm.) yields two age populations. The younger population has an age of 121 ± 15 Ma, which is similar to the Aptian–Albian stratigraphic age of the formation (determined using microfossils [10]). However, a morphologically distinct population of older zircons yields an older age of 347 ± 27 Ma (Table 2).

4. Interpretation and discussion

4.1. Periods of cooling north of 1°30′S

In order to extract thermal history information from the $^{40}Ar/^{39}Ar$ data, estimates of the closure temperatures (T_c) of each mineral phase to the K/Ar system have been made utilising experimentally defined diffusion parameters (e.g. [23]). We have no a priori knowledge of palaeo-cooling rates within the study area. Therefore, the bulk T_c values for hydrous white mica and biotite phases have been calculated [24] for a large spread of cooling rates of 50–10°C/Myr and range be-

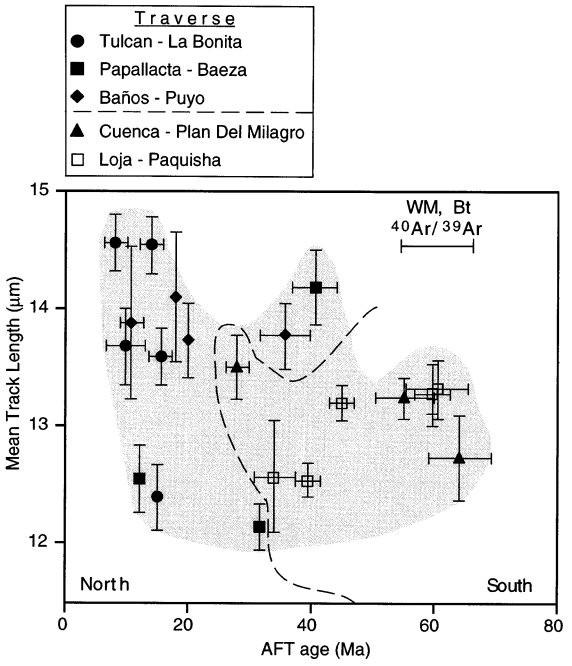

Fig. 4. AFT age versus mean fission-track length for those samples from the Cordillera Real that yielded sufficient length data (including data from Spikings et al. [18]). The dashed line separates those samples located north of 1°30′S from those located south of 2°45′S.

tween ~380 and 350°C and 350 and 325°C, respectively.

Spikings et al. [18] presented several modelled temperature–time envelopes that described the most likely thermal histories of regions of the Cordillera Real north of 1°30′S at temperatures ≤110°C. The modelling followed the approach of Gallagher [25], using the quantitative description of AFT annealing kinetics described by Laslett et al. [26]. The envelopes were defined by grouping together the 50 temperature–time paths, which yielded predicted AFT data that most closely matched the observed AFT data. Where ZFT ages were available, the envelopes were extrapolated to a temperature of 260°C, which lies at the mid-point of the temperature zone where tracks are partially annealed in zircon (samples 98RS55, 98RS28 and 98RS14) [18,27]. Fig. 5 shows the results of combining some of those models with the $^{40}Ar/^{39}Ar$ data acquired in this study. The close similarity of the $^{40}Ar/^{39}Ar$ white mica and biotite ages (65–55 Ma; Fig. 2) over a potential temperature range of 380–325°C suggests that they record a distinctive cooling event during 65–55 Ma. In addition, previously measured and un-interpreted ZFT ages (zone of partial track annealing in zircons is between 300 and 220°C; [27]) of ~60 Ma along traverses between the towns of Papallacta and Baeza and between Baños and Puyo (Fig. 2; [18]) are interpreted here to record the lower temperature segment of the same cooling event (e.g. 98RS14; Fig. 5). AFT ages north of 1°30′S range between ~40 and 10 Ma and this region did not cool to temperatures <110°C until at least ~43 Ma. Rocks in the northern Cordillera Real cooled rapidly to temperatures ≤110°C at rates as high as 30°C/Myr, probably via crustal exhumation, during ~43–30 Ma, 25–15 Ma and 10–0 Ma (Fig. 5; [18]). The amount of cooling and exhumation recorded at any particular time varies between sample locations. However, ZFT and AFT ages from between the towns of Tulcan and La Bonita in far northern Ecuador fall within a narrow range of ~15–8 Ma (Figs. 1 and 2) and this region has cooled significantly more (up to 200°C) than regions further south since ~15 Ma (Fig. 5).

The Jurassic biotite $^{40}Ar/^{39}Ar$ age from far northern Ecuador (sample 98RS55; 162±2 Ma) is from a faulted slice of deformed rhyolites of the Misahualli Volcanic Unit and is distinctly older than other $^{40}Ar/^{39}Ar$ ages recorded in this study. However, the same sample yields concordant ZFT and AFT ages of ~15 Ma [18] and experienced rapid cooling from temperatures of ~260 to <80°C at ~15 Ma. The extrusion age of the Misahualli Volcanic Unit is not well known although K/Ar ages from further south record ages varying between ~168 and 143 Ma, which led Litherland et al. [10] to define the unit as containing Jurassic continental volcanic rocks. Therefore, we propose that the biotite $^{40}Ar/^{39}Ar$ age reported here is a result of rapid cooling following the eruption. Subsequent burial was insufficient to reset the biotite K/Ar system (< ~325°C) but high enough to remove pre-existing fission-tracks in the zircon grains. Therefore, the $^{40}Ar/^{39}Ar$ age of 162±2 Ma is consid-

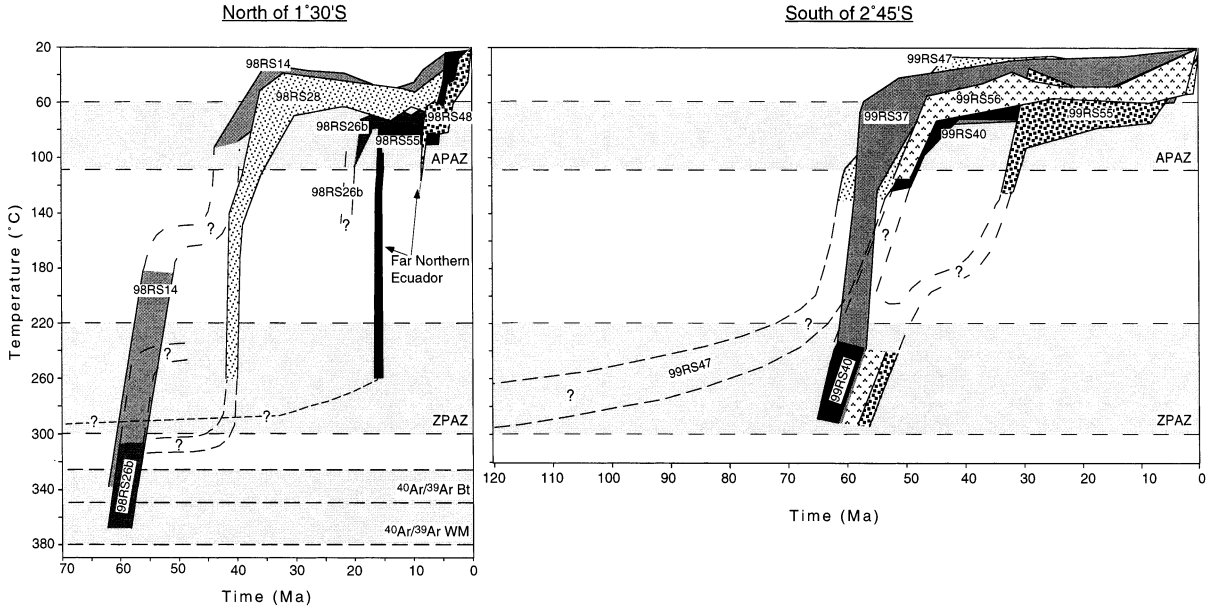

Fig. 5. Temperature–time envelopes for representative samples north of 1°30′S and south of 2°45′S. Each envelope was produced by modelling the AFT data [25,26] and combining the result with concordant (same ages within error) white mica and biotite $^{40}Ar/^{39}Ar$ and ZFT track ages. Temperature–time envelopes are only shown for those samples which yielded the most amount of data (i.e. both $^{40}Ar/^{39}Ar$ and fission-track data) and the most precise data (i.e. more than 50 fission-track length measurements). For the fission-track systems, the shaded zones show the region where tracks partially anneal in apatite [26] and zircon [27]. For the $^{40}Ar/^{39}Ar$ system, the shaded zone is that defined by the range of closure temperatures for cooling rates between 10 and 50°C/Myr. APAZ: apatite partial annealing zone, ZPAZ: zircon partial annealing zone, Bt: biotite, WM: white mica.

ered to be a minimum extrusion age for rhyolite 98RS55.

4.2. Periods of cooling south of 2°45′S

AFT ages from south of 2°45′S range between 64 and 11 Ma (Table 2; Fig. 2) suggesting that the present land surface was variably cooling through the ~110°C isotherm during and prior to this time period. All of the track lengths are partially annealed (< ~14.5 μm) although a cluster of relatively long lengths occurs at ~60–55 Ma (Fig. 4). The AFT data for those samples with more than 50 track length measurements has been modelled (e.g. [18]) to quantify the timing and amount of cooling at specific sample locations at temperatures ≤110°C. Modelling followed the approach of Gallagher [25], using the quantitative description of AFT annealing kinetics described by Laslett et al. [26]. Most of the ZFT ages range between 63 and 33 Ma (Fig. 2) and these have been combined with the AFT thermal models where ZFT and AFT data exists for the same sample to generate the temperature–time envelopes shown in Fig. 5. The partial retention zone for fission-tracks is generally considered to lie between ~300 and 220°C for zircons [27] and between ~110 and 60°C for apatites of commonly occurring compositions. Deviations from these limits can occur within compositionally exotic phases; more in-depth discussions of track annealing kinetics are presented elsewhere (e.g. [28]).

Most of the modelled samples, from both the Cordillera Real (99RS37, 99RS40, 99RS56) and the SAZ (99RS47), cooled at elevated rates during the period spanning 65–45 Ma and were at temperatures ≤60°C by 40 Ma. Higher average cooling rates of up to ~20°C/Myr are calculated for the period 65–55 Ma (cooling from 260 to 60°C). However, several samples yield AFT ages younger than 40 Ma (e.g. 99RS55; Fig. 2) and were cooling through ~110°C at ~35–30 Ma (Fig. 5).

99RS53 is the only sample from south of 2°45′S that yields a Miocene AFT age (11 ± 1 Ma; Table 2; Fig. 3) and cooled through the ~110°C isotherm significantly later than other samples from this region.

Several ZFT ages from south of 2°45′S are older than the $^{40}Ar/^{39}Ar$ and fission-track ages from all other sampled regions (Table 2; Fig. 2). ZFT ages from the Zamora Batholith (131–101 Ma) post-date its crystallisation age (190–170 Ma; [10]) by at least 40 Myr and are probably mixed ages that were partially reset by pre-Cenozoic as well as Cenozoic cooling events that cannot be quantified with the current data set. Metasediments 99RS38, 39 and 52, of the Palaeozoic Chiguinda Unit contain older zircon populations, which can be statistically distinguished from younger populations within the same sample (Table 2). The ages of the older populations from these samples range between 94 and 13 Ma and 463 and 160 Ma and have not been totally reset by Cenozoic events. The zircons in these populations are more rounded and darker, suggesting they were derived from a distinctly different and probably older source region than the more pristine zircon crystals that yield Cenozoic ZFT ages. They may also be compositionally distinct from the younger zircon population and may require higher track annealing temperatures, accounting for the preservation of older ZFT ages. The form of the pre-Cenozoic *T–t* path cannot be derived for any of the older populations.

4.3. Along-strike thermal history variations and their relation to the contemporaneous oceanic domain

4.3.1. 65–30 Ma

The thermal history paths derived in this study show that the entire Ecuadorian Cordillera Real experienced two pulses of cooling, which occurred at similar rates during ~65–30 Ma. Concordant white mica, biotite and ZFT ages, as well as modelling of AFT track data suggests that cooling rates increased during 65–55 Ma and at ~43–30 Ma (Figs. 4 and 5). Evidence for the cooling history from temperatures lower than ~300°C from far northern Ecuador (between the towns of Tulcan and La Bonita) has been lost by erosion and therefore cooling during 65–30 Ma in that location cannot be confirmed with the current data set.

Continental red beds of the Tena Fm., were deposited to the east of the Cordillera Real within the developing Amazon Foreland Basin during the Maastrichtian–Palaeocene (72–57 Ma) and were the first rocks to be sourced from the Cordillera Real [29], suggesting that the Cordillera was uplifting at this time. In support of this, Litherland et al. [11] attribute reset and mixed muscovite and biotite K/Ar ages (90–50 Ma, e.g. [10,30]), from pre-Cretaceous schists of the Loja and Salado Terranes to resetting caused by shearing and heating during a Late Cretaceous–Early Tertiary metamorphic event. This loosely constrained period may also have caused the Cordillera Real to be uplifted [10]. At a similar time, turbidites of the Yunguilla Unit were being partly shed off to the west from the Cordillera Real and deposited on oceanic crust of the Pallatanga Terrane [12] during the Maastrichtian. Based on this information, Hughes and Pilatasig [12] suggest the Pallatanga Terrane accreted against the continent during the Campanian (83–74 Ma) along the Pujili Fault (Fig. 1).

The Late Eocene accretion of the composite Piñon–Macuchi Block along the Chimbo–Toachi Shear Zone is more tightly constrained by a depositional unconformity that spans the Late Eocene–Miocene period [31]. Furthermore, subsequent changes in the composition of volcanic rocks, as well as a K/Ar age of sheared hornblendes from an intrusion within the Chimbo–Toachi Shear Zone of ~48 Ma may represent the earliest stage of dextral shearing [12] associated with this accretionary phase.

Within Colombia, Late Cretaceous thrusting and metamorphism of the Early Cretaceous oceanic Calima and continental Tahami terranes and the Campanian accretion of the Amaime Terrane [2,14,15] was synchronous with the accretion of the Pallatanga Terrane in Ecuador (Fig. 1). Late Cretaceous extrusion ages of basalts in the Pallatanga Terrane [12] and the oceanic Calima Terrane in Colombia [32], are similar to those of the Caribbean Plateau [33]. Furthermore, geochemi-

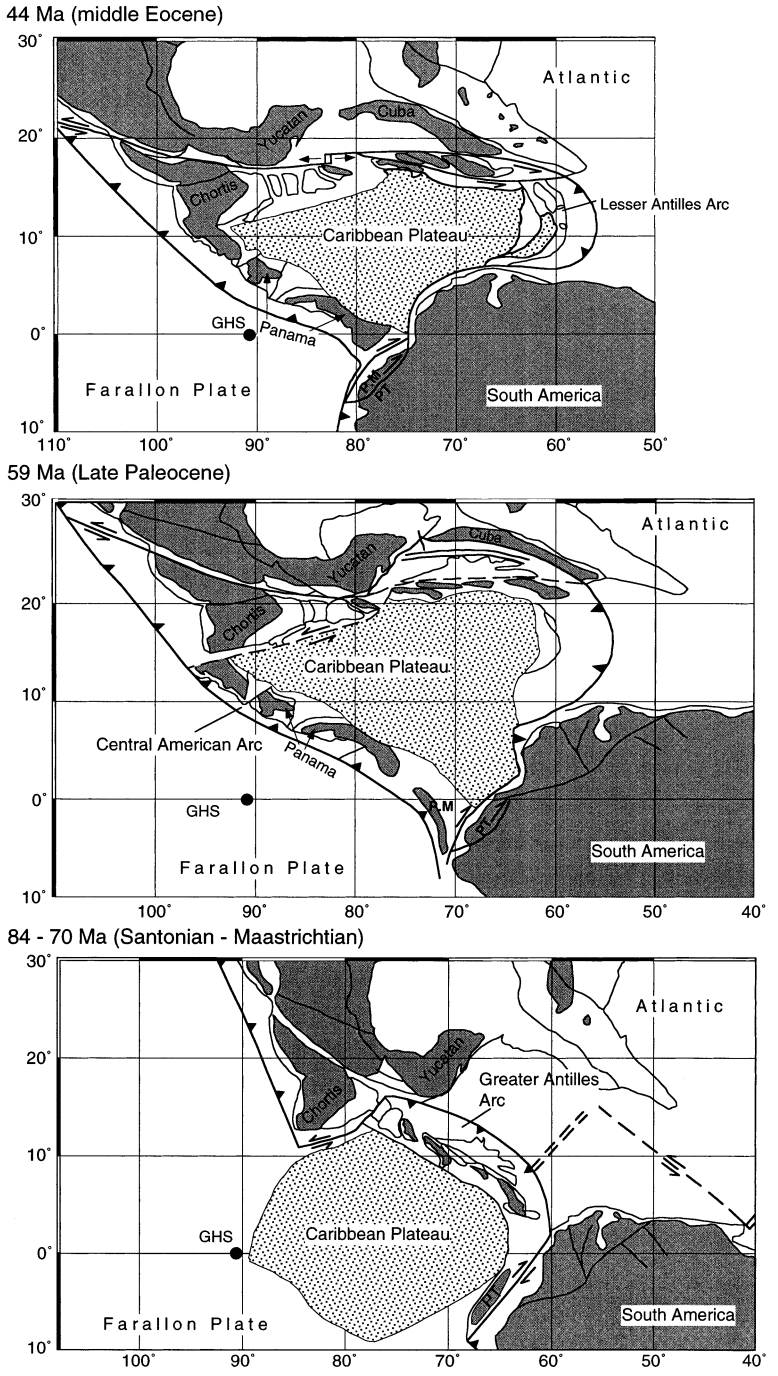

Fig. 6. Reconstruction of the Caribbean Plateau from 84 to 44 Ma (modified from [35]). GHS: Galapagos Hot Spot. Schematic postulated extensions to the Great Arc of the Antilles and the Central American Arc have been made to include the Piñon–Macuchi Block (P.M) and the Pallatanga Terrane (PT).

cal signatures of basement basalts of the Pallatanga Terrane and the Caribbean Plateau are similar [34]. These similarities, combined with plate reconstructions that assume the Caribbean Plateau formed over the Galapagos Hot Spot and subsequently drifted to its current position (e.g. [35]), suggest that the allochthonous basement of northwestern South America may have been at least partly derived from the Caribbean Plateau. The timing of accretion suggests that the present day Pallatanga and Calima terranes may have been derived from the southern segment of the Great Arc of the Antilles (e.g. [36]), which collided with the leading edge of the approaching Caribbean Plateau at ~84–70 Ma (Fig. 6). Furthermore, we suggest that pre-accretionary formations of ocean island arc affinity within the Piñon–Macuchi Block (e.g. [12]) may have originally been part of the trailing Costa Rica/Panama ocean island arc of the Caribbean Plateau that now forms much of Central America (Fig. 6).

Isostatic re-equilibration following a compressive and probably crustal thickening period will prolong the duration of elevated exhumation rates beyond the period of peak compressive stress during a collision event. Therefore, the periods of accelerated cooling identified here (65–55 and 43–30 Ma) were probably driven by the accretion of the Pallatanga Terrane and the Piñon–Macuchi Block to the continental margin, but post-date the regional maximum compressive stress by <10 Myr (e.g. [37]). In addition, subduction of oceanic crust beneath the leading edge of the Caribbean Plateau began between ~84 and 70 Ma [36] and may have increased regional geothermal gradients prior to the increased Late Cretaceous–Palaeocene (65–55 Ma) cooling rates identified here. Therefore, a component of the cooling may be a consequence of thermal relaxation from a higher temperature thermal regime that started to cool within Ecuador at ~65 Ma.

A paucity of palaeo-magnetic and precise structural data renders it difficult to reconstruct the relative position of the NW SOAM margin and the allochthonous blocks at the time of these collision events. Shear indicators in the Pujili Fault and the Chimbo–Toachi Shear Zone suggest a dextral sense of movement [12], possibly driven by the east-northeastward displacement of the Caribbean Plateau into its current position relative to South America. Dextral displacement of the oceanic region towards the northeast, utilising the Pallatanga [38] and La Sofia faults [39] persists today at a rate of ~1 cm/yr [16]. Assuming a constant displacement rate, the measured slip rate is equivalent to 150 km northeastward movement since the middle Miocene. Therefore, it is likely that the oceanic terranes accreted against South America further south than their current position, possibly somewhere in the vicinity of the Huancabamba Deflection (Fig. 1). The accretion events drove increased cooling rates, probably via erosional exhumation, along the entire contemporaneous Ecuadorian margin both during the Palaeocene and Eocene–early Oligocene.

4.3.2. 30–0 Ma

From 30 Ma to present, most of the Cordillera Real north of 1°30′S cooled significantly more and was exhumed from greater depths than the region south of 2°45′S after 30 Ma (Fig. 5). Thermal relaxation following Oligocene volcanism combined with increased rates of crustal exhumation generated particularly high cooling rates in the north during 23–15 Ma (12–50°C/Myr) and 10–0 Ma ($\leq$50°C/Myr; [18]). South of 2°45′S, the 23–15 Ma cooling 'event' is generally not observed and any cooling that occurred after 10 Ma was at slower rates than that experienced north of 1°30′S (Fig. 5). Furthermore, within the region north of 1°30′S, far northern Ecuador experienced distinctly higher cooling and exhumation rates both at ~15 Ma ($\leq$50°C/Myr) and since ~10 Ma than more southern regions (Fig. 5; [18]). These distinct along-strike differences in cooling and exhumation histories since 30 Ma correlate closely with heterogeneities in the subducting oceanic plate, as well as increasing convergence rates between the Nazca and SOAM plates during ~25–20 Ma [8].

At the present day the subducted Nazca Plate between the Malpelo Fossil Rift and the Grijalva Fracture Zone is composed of the Carnegie Ridge, oceanic crust younger than 25 Myr old and the Grijalva Fracture Zone system that delimits Nazca crust (<25 Ma) from the older Far-

allon Crust (>25 Ma; Fig. 1). Within the same region, the sea floor is up to 2km shallower than regions to the north and south [6,40]. Modern seismicity patterns combined with the trend of adakitic [41] and other active volcanic centres lead Gutscher et al. [6] to propose that the buoyant Carnegie Ridge extends beneath the SOAM margin with a flat-slab geometry. Their proposed limits, which separate the flat-slab from steeper subducting slab segments via lithospheric tears are shown in Fig. 1 and may extend up to 500 km inland from the trench. At present, the southern limit of the flat-slab segment is located at ~1°S within the Cordillera Real, whilst its northern limit is at ~3°N [6]. Within Ecuador, this corresponds with the younger cooling history observed to the north of 1°30′S revealed through the fission-track data in the present study. Furthermore, the youngest AFT ages, generated by deeper levels of exhumation since ~15 Ma, are located directly above the proposed crest of the ridge (Fig. 1).

The timing of collision of the Carnegie Ridge with the North Andean margin has been a matter of conjecture for over 20 yr. The opinion of, for example, Lonsdale and Klitgord [40] that underthrusting has been occurring since only ~1–3 Ma generally prevails in the literature. However, more recent lines of evidence suggest that collision occurred earlier. These are:

1. Variations in coastal morphology, generated by the southward migration of the Carnegie Ridge led Gutscher et al. [6] to propose that the Carnegie Ridge collided with the trench since 8 Ma, and caused the northeastward drift of the allochthonous oceanic terranes at rates of 1–2 cm/yr [42].
2. On the basis of seismicity patterns, Gutscher et al. [6] showed that the Carnegie Ridge can be traced at least 120–500 km east of the trench beneath the continental plate, which at current plate convergence rates (Fig. 1) implies that collision occurred prior to 3 Ma.
3. Lonsdale and Klitgord, [40] assumed very low mean plate convergence rates of 55 mm/yr [43] between the Nazca Plate and the northern SOAM continent.
4. Late Miocene–Pliocene uplift, recorded by shallowing upward trends in the Ecuadorian forearc (Manabi and Progreso basins) within the western Piñon–Macuchi Block led Daly [44] to propose that the initial collision occurred at ~8 Ma.

Global plate reconstructions [7,8,17] show that the Nazca Plate has converged almost orthogonally with the SOAM Plate at rates as high as ~120 mm/yr since the break-up of the Farallon Plate at 25 Ma. The eastward push from the East Pacific Rise, combined with north–south oriented spreading along the Malpelo and Galapagos rifts has given rise to the bifurcation of the Cocos and Carnegie ridges, which formed over the Galapagos Hot Spot (Fig. 1). Plateau basalts of the Galapagos Hot Spot rest upon oceanic crust of the Nazca Plate, which has been dated at ~22 Ma (Fig. 1; [40,45]) and may be used as a minimum reference starting time for eastward movement of the Carnegie Ridge. However, other workers proposed that the Galapagos Hot Spot may have driven the break-up of the Farallon Plate (e.g. [43]) at ~25 Ma.

Plate convergence rate calculations [7,8,17] for the time spanning 25–20, 20–10 and 10–0 Ma are 50–150 (the higher rate is recorded at 12°S), 80–140 and 57–80 mm/yr, respectively. Radiogenic and micropalaeontologic dating of Carnegie Ridge basalts [46] and their overlying sediments, respectively (DSDP site 157l; Fig. 1; [47]), suggest that the Carnegie Ridge has drifted eastwards at a rate of 67–75 mm/yr since 9 Ma [46], which compares well with proposed rates [7,8,17] for the same time interval. Utilising the minimum and maximum convergence rates since 22 Ma [8], the Carnegie Ridge would have collided with the Ecuador Trench at some time between 15 and 9 Ma, respectively. Within Ecuador, this time period coincides with the development of the Manabi and Progreso pull-apart basins over the coastal region (Fig. 1; e.g. [44]) and extension in southern Ecuador causing shallow marine ingressions into the southern Inter-Andean valley during 15–10 Ma [48]. These have been attributed to the north-northeast directed dextral displacement of the allochthonous oceanic blocks since 15 Ma

[49,50], which removed the crustal support for the hinterland to the east of the present day Gulf of Guayaquil, resulting in extension and collapse. The same tectonic rearrangement is probably responsible for a sudden increase in exhumation rates in far northern Ecuador at ~15 Ma. Collision of the anomalously thick and buoyant Carnegie Ridge at ~15 Ma may have provided the driving force for the northeastward displacement, causing extension and subsidence in the south during 15–10 Ma [48] and compression and uplift in the north.

The restriction of rapid exhumation rates to the north is consistent with higher and more juvenile land surfaces composed of metamorphic rocks (excluding the Quaternary and Recent >5000 m high volcanic peaks), which have been uplifted by the Carnegie Ridge collision north of ~2°45′S (Fig. 1). The elevated landscape swings seaward in the vicinity of the Gulf of Guayaquil, crossing major fault zones such as the Peltetec Fault and is approximately parallel with the Grijalva Fracture Zone and the previously proposed lithospheric tears (Fig. 1; [6]). This trend suggests that there is a deep crustal influence on the evolving topography.

Elevated cooling rates commencing at ~9 Ma are commonly recorded north of 1°30′S (Fig. 5) and cooling at this time is probably also partly responsible for the single Upper Miocene AFT age from south of 2°45′S (99RS53; 11±1 Ma). Cooling at this time may be a result of increased exhumation rates that were driven by an increase in compressive stress and buoyancy of the continental margin, which developed as a consequence of coupling between the continental crust and the subducting flat-slab of the Carnegie Ridge.

5. Conclusions

The location of along-strike variations in the Cenozoic thermal history of the Cordillera Real are consistent with the collision and subduction of contemporary heterogeneities (varying crustal age, density and thickness) in the approaching oceanic plate.

1. The collision of ocean island arcs that may have developed at the boundaries of the Caribbean Plate with the SOAM continent affected the entire margin of the Northern Andean Segment (north of 5°S) as far south as southernmost Ecuador. These collision events resulted in elevated cooling rates of up to 20°C/Myr in the Cordillera Real during extended time periods of 65–55 and 43–30 Ma.
2. The role of the Carnegie Ridge in the post-middle Miocene thermochronological and exhumational history of Ecuador seems to have been of paramount importance. Northern Ecuador (north of 1°30′S) has experienced significantly more cooling and exhumation since ~30 Ma than the region south of 2°45′S. Collision of the Carnegie Ridge with the Ecuadorian Trench at ~15 Ma resulted in elevated cooling and exhumation rates in the north at ~15 Ma and extension in the south. Subsequent flat-slab coupling of the Carnegie Ridge with the continental plate may have caused isostatic disequilibrium and a compressional stress regime, resulting in significantly increased exhumation rates since 9 Ma. Lithospheric tears and steeper slab subduction, together with reactivation of shear zones separating continental from oceanic basement may have isolated southern Ecuador from the compressive regime that prevailed in the north.
3. The elevated topography in northern Ecuador swings seaward in the vicinity of the Gulf of Guayaquil and is approximately parallel with the Grijalva Fracture Zone and the location of previously proposed lithospheric tears [6], suggesting a deep crustal influence on the evolving topography. The most juvenile land surfaces lie directly above the proposed extent of the crest of the subducted ridge.

Acknowledgements

The authors would like to express their thanks to Richard Hughes and Kevin Burke for several useful discussions on the configuration and reconstruction of western Ecuador and the Caribbean region, respectively. Field sampling benefited from

the assistance and support of Diego Villagomez (EPN-Quito). The manuscript was improved by the thorough and careful reviews of James Kellogg and Barry Kohn. Funding for the project was provided by the Swiss National Science Foundation, project numbers 21-050844.97 and 20-56794-99.*[SK]*

References

[1] A. Gansser, Facts and theories on the Andes, J. Geol. Soc. Lond. 129 (1973) 93–131.
[2] 2 J.L. Pindell, K.D. Tabutt, Mesozoic–Cenozoic Andean palaeogeography and regional controls on hydrocarbon systems, in: A.J. Tankard, R. Suarez, H.J. Welsink (Eds.), Petroleum Basins of South America, AAPG Memoir 62 (1995) 101-128.
[3] E.R. Engdahl, R.D. Van der Hilst, R. Buland, Global teleseismic earthquake rotation with improved travel times and procedures for depth location, Bull. Seismol. Soc. Am. 88 (1998) 722–743.
[4] M.L. Hall, C.A. Wood, Volcano-tectonic segmentation of the northern Andes, Geology 13 (1985) 203–207.
[5] J. Vanek, V. Vankova, V. Hanus, Geochemical zonation of volcanic rocks and deep structure of Ecuador and southern Colombia, J. S. Am. Earth Sci. 7 (1994) 55–67.
[6] M.-A. Gutscher, J. Malavieille, S. Lallemand, J.-Y. Collot, Tectonic segmentation of the North Andean margin: impact of the Carnegie Ridge collision, Earth Planet. Sci. Lett. 168 (1999) 255–270.
[7] R.H. Pilger, Cenozoic plate kinematics subduction and magmatism: South American Andes, J. Geol. Soc. London 141 (1984) 793–802.
[8] F. Pardo-Casas, P. Molnar, Relative motion of the Nazca (Farallon) and South America plate since late Cretaceous time, Tectonics 6 (1987) 233–248.
[9] E. Jaillard, T. Sempéré, P. Soler, G. Carlier, R. Marocco, The role of Tethys in the evolution of the northern Andes between Late Permian and Late Eocene times, in: A.E.M. Nairn et al. (Eds.), The Ocean Basins and Margins, vol. 8, Plenum Press, New York, 1995, pp. 463–491.
[10] M. Litherland, J. Aspden, R.A. Jemielita, The metamorphic belts of Ecuador, British Geological Survey, Overseas Memoir 11, 1994, p. 147.
[11] F. Davila, A. Egüez, Deformation analysis in the basement of the Chota Basin: Ambaqui Group, Bol. Geol. Ecuat. 1 (1990) 39–52.
[12] R.A. Hughes, L.F. Pilatasig, Cretaceous and Tertiary terrane accretion in the Cordillera Occidental of the Ecuadorian Andes, in: Fourth International Symposium on Andean Geodynamics (ISAG), Göttingen, Germany, 1999, pp. 340–342.
[13] T. Feininger, M.K. Seguin, Simple Bouger gravity anomaly field and the inferred crustal structure of continental Ecuador, Geology 11 (1983) 40–44.
[14] W.J. McCourt, J.A. Aspden, M. Brook, New geological and geochronological data from the Colombian Andes: continental growth by multiple accretion, J. Geol. Soc. Lond. 141 (1984) 831–845.
[15] J.F. Toussaint, J.J. Restrepo, The Colombian Andes during Cretaceous times, in: J.A. Salfity (Ed.), Cretaceous Tectonics of the Andes, Braunschweig, Wiesbaden, Germany, 1994, pp. 61–100.
[16] J.N. Kellogg, V. Vega, Tectonic development of Panama, Costa Rica, and the Colombian Andes: constraints from global positioning system geodetic studies and gravity, Geol. Soc. Am. Spec. Pap. 295 (1995) 75–90.
[17] E.O. Norabuena, T.H. Dixon, S. Stein, C.G.A. Harrison, Decelerating Nazca–South America and Nazca–Pacific plate motions, Geophys. Res. Lett. 26 (1999) 3405–3408.
[18] R.A. Spikings, D. Seward, W. Winkler, G.M. Ruiz, Low-temperature thermochronology of the northern Cordillera Real, Ecuador tectonic insights from zircon and apatite fission-track analysis, Tectonics 19 (2000) 649–668.
[19] I. McDougall, T.M. Harrison, Geochronology and Thermochronology by the $^{40}Ar/^{39}Ar$ Method, Oxford University Press, New York, 1999.
[20] R.H. Steiger, E. Jäger, Subcommission on geochronology: convention on the use of decay constants in geo- and cosmochronology, Earth Planet. Sci. Lett. 36 (1977) 359–362.
[21] A. Burghele, Propagation of error and choice of standard in the ^{40}Ar-^{39}Ar technique, Chem. Geol. 66 (1987) 17–19.
[22] R.F. Galbraith, P.F. Green, Estimating the component ages in a finite mixture, Nucl. Tracks Rad. Meas. 17 (1990) 197–206.
[23] T.M. Harrison, I. Duncan, I. McDougall, Diffusion of ^{40}Ar in biotite: temperature, pressure and compositional effects, Geochim. Cosmochim. Acta 49 (1985) 2461–2468.
[24] M.H. Dodson, Closure temperature in cooling geochronological and petrological systems, Contrib. Miner. Petrol. 40 (1973) 259–274.
[25] K. Gallagher, Evolving thermal histories from fission-track data, Earth Planet. Sci. Lett. 136 (1995) 421–435.
[26] G.M. Laslett, P.F. Green, I.R. Duddy, A.J.W. Gleadow, Thermal annealing of fission tracks in apatite 2: a quantitative analysis, Chem. Geol. 65 (1987) 1–15.
[27] T. Tagami, R.F. Galbraith, R. Yamada, G.M. Laslett, Revised annealing kinetics of fission tracks in zircon and geological implications, in: P. Van den Haute, F. de Corte (Eds.), Advances in Fission-Track Geochronology, Solid Earth Sciences Library 10, Kluwer Academic, Norwell, 1998, pp. 99–112.
[28] W.D. Carlson, R.A. Donelick, R.A. Ketcham, Variability of apatite fission-track annealing kinetics: I. Experimental results, Am. Miner. 84 (1999) 1213–1223.
[29] M.W. Baldock, Geology of Ecuador, explanatory bulletin of the national geological map of the Republic of Ecuador 1:1 000 000 scale, Rev. Dir. Gen. Geol. Minas Ecuador, Inst. Geol. Sci., London, 1982.

[30] H.J. Herbert, H. Pichler, K–Ar ages of rocks from the Eastern Cordillera of Ecuador, Z. Dtsch. Geol. Ges. 134 (1983) 483–493.
[31] R.A. Hughes, R. Bermudez, Geology of the Cordillera Occidental of Ecuador between 0°00′ and 1°00′S, Proyecto de Desarollo Minero y Control Ambiental, Program. Inform. Cartograf. Geol., Informe 4, Dirrecion Nacional de Geologica, Quito Ecuador.
[32] J.A. Aspden, W.J. McCourt, M. Brook, Geometrical control of subduction-related magmatism: the Mesozoic and Cenozoic plutonic history of Western Colombia, J. Geol. Soc. Lond. 144 (1987) 893–905.
[33] C.W. Sinton, R.A. Duncan, M. Storey, J. Lewis, J.J. Estrada, An oceanic flood basalt province within the Caribbean plate, Earth Planet. Sci. Lett. 155 (1998) 221–235.
[34] M. Mamberti, D. Bosch, H. Lapierre, J. Hernandez, E. Jaillard, M. Polve, Petrology and geochemistry of Mg-rich basalts from Western Ecuador: remnants of the Late Cretaceous Caribbean Plateau, in: Fourth International Symposium on Andean Geodynamics (ISAG), Göttingen, Germany, 1999, pp. 832–835.
[35] M.I. Ross, C.R. Scotese, A hierachial tectonic model of the Gulf of Mexico and Caribbean region, Tectonophysics 155 (1988) 139–168.
[36] K. Burke, Tectonic evolution of the Caribbean, Ann. Rev. Earth Planet. Sci. 16 (1988) 201–230.
[37] E.A. Keller, N. Pinter, Active Tectonics: Earthquakes, Uplift and Landscape, Upper Saddle River, New Jersey, Prentice-Hall, Englewood Cliffs, NJ, 1996.
[38] T. Winter, J.-P. Avouac, A. Lavenu, Late Quaternary kinematics of the Pallatanga strike–slip fault (Central Ecuador) from topographic measurements of displaced morphological features, Geophys. J. Int. 115 (1993) 905–920.
[39] F. Ego, M. Sebrier, A. Lavenu, H. Yepes, A. Eques, Quaternary state of stress in the northern Andes and the restraining bend model for the Ecuadorian Andes, Tectonophysics 259 (1996) 101–116.
[40] P. Lonsdale, P.D. Klitgord, Structure and tectonic history of the eastern Panama Basin, Geol. Soc. Am. Bull. 89 (1978) 981–999.
[41] M. Monzier, C. Robin, M.L. Hall, J. Cotton, P. Mothes, J.-P. Eissen, P. Samaniego, Les adakites d'Equateur: modèle préiliminarie, C. R. Acad. Sci. Paris 324 (1997) 545–552.
[42] J.T. Freymueller, J.N. Kellogg, V. Vega, Plate motions in the North Andean region, J. Geophys. Res. 98 (1993) 21853–21863.
[43] R.N. Hey, Tectonic evolution of the Cocos–Nazca spreading center, Geol. Soc. Am. Bull. 88 (1977) 1414–1420.
[44] M.C. Daly, Correlations between Nazca/Farallon plate kinematics and forearc basin evolution in Ecuador, Tectonics 8 (1989) 769–790.
[45] M. Meschede, W. Frisch, A plate tectonic model for the Mesozoic and early Cenozoic history of the Caribbean Plate, Tectonophysics 296 (1998) 269–291.
[46] D.M. Christie, R.A. Duncan, A.R. McBirney, M.A. Richard, W.M. White, K.S. Harpp, C.G. Fox, Drowned island downstream from the Galapagos hotspot implying extended speciation times, Nature 355 (1992) 246–248.
[47] T.H. Van Andel, G.R. Heath, R.H. Bennett, J.D. Bukry, S. Charleston, D.S. Cronan, M.G. Dinkelman, A.G. Kaneps, K.S. Rodolfo, R.S. Yeats, Initial Rep. Deep Sea Drill. Proj. 16 (1971) 54–61.
[48] M. Steinmann, D. Hungerbühler, D. Seward, W. Winkler, Neogene tectonic evolution and exhumation of the southern Ecuadorian Andes: a combined stratigraphy and fission-track approach, Tectonophysics 307 (1999) 255–276.
[49] G.L. Shepherd, R. Moberly, Coastal structure of the continental margin, northwest Peru and southwest Ecuador, in: L. Kulm, J. Dymond, E.J. Dasch, D.M. Hussong (Eds.), Nazca Plate: Crustal Formation and Andean Convergence, Geol. Soc. Am. Mem. 154, 1981, pp. 351–391.
[50] D. Hungerbühler, Neogene Basins in the Andes of Southern Ecuador: Evolution, Deformation and Regional Tectonic Implications, Ph.D. thesis, Eidg. Tech. Hochsch., Zürich, 1997.